Research Square

Preprints are preliminary reports that have not undergone peer review.
They should not be considered conclusive, used to inform clinical practice,
or referenced by the media as validated information.

Multi-Pass Focused Helium Ion Beam Processing for Reducing Ga-FIB-Induced Surface Damage in Single-Crystal Diamond

Yisen Chen
Guangdong University of Technology
Yun Zheng
Guangdong University of Technology
FengLing Zou
Guangdong University of Technology
Zelong Lin
Guangdong University of Technology
Chengyong Wang
Guangdong University of Technology
Lijuan Zheng
Guangdong University of Technology
Zhishan Yuan
zhishanyuan@gdut.edu.cn
Guangdong University of Technology

Research Article

Keywords: Diamond, Focused gallium ion beam, Helium ion microscopy, Surface damaged layer, Multi-pass processing

Posted Date: November 23rd, 2026

DOI: https://doi.org/10.21203/rs.3.rs-11426116/v1

License: This work is licensed under a Creative Commons Attribution 4.0 International License.
Read Full License

Additional Declarations: No competing interests reported.

Multi-Pass Focused Helium Ion Beam Processing for Reducing Ga-FIB-Induced Surface Damage in Single-Crystal Diamond

Yisen Chen [1,2,3,4]†, Yun Zheng[1,2,3,4]†, FengLing Zou [1,2,3,4], Zelong Lin [1,2,3,4] , Chengyong Wang[1,2,3,4],Lijuan Zheng[1,2,3,4], Zhishan Yuan[1,2,3,4*]

[1]School of Electro-Mechanical Engineering, Guangdong University of Technology, Guangzhou 510006, China

[2]Guangdong Provincial Key Laboratory of Minimally Invasive Surgical Instruments and Manufacturing Technology, Guangdong University of Technology, Guangzhou 510006, China

[3]State Key Laboratory of High-Performance Tools, Guangdong University of Technology, Guangzhou 510006, China

[4]Smart Medical Innovation Technology Center, Guangdong University of Technology, Guangzhou 510006, China

* Corresponding author: zhishanyuan@gdut.edu.cn;

†These authors contributed equally to the work and should be regarded as co-first authors.

Abstract

Single-crystal diamond has attracted considerable attention for applications in quantum information processing, nanophotonics, and microelectromechanical systems. However, focused gallium ion beam (Ga-FIB) milling introduces near-surface structural damage and gallium implantation, which may adversely affect the performance of diamond-based nanostructures. In this study, focused helium ion beam (He-HIM) post-processing was investigated as a potential approach for reducing Ga-FIB-induced surface damage in single-crystal diamond. The effects of helium ion dose, beam current, and multi-pass processing conditions on the damaged-layer thickness were systematically examined using cross-sectional transmission electron microscopy (TEM), high-resolution TEM (HRTEM), energy-dispersive X-ray spectroscopy (EDS), and selected-area electron diffraction (SAED). The results showed that helium ion irradiation at a dose of 5×10^{15} ions/cm² reduced the local damaged-layer thickness from 200.39 ± 1.46 nm to 192.97 ± 1.06 nm, whereas higher doses resulted in increased damaged-layer thickness. Beam-current experiments revealed that regions processed at 13–29.67 pA exhibited thicker damaged layers than the 12 pA reference regions, although no monotonic dependence on beam current was observed. Based on these findings, two six-pass He-HIM processing strategies were implemented using progressively reduced beam currents or ion doses. Compared with corresponding Ga-FIB-only reference regions, the multi-pass treatments reduced the local damaged-layer thickness by approximately 5.6% and 8.0%, respectively. These findings suggest that carefully controlled He-HIM post-processing can moderately reduce Ga-FIB-induced surface damage, while excessive irradiation may introduce additional structural defects. This study provides experimental guidance for optimizing helium ion beam post-processing of diamond nanostructures.

Keywords: Diamond; Focused gallium ion beam; Helium ion microscopy; Surface damaged layer; Multi-pass processing.

1. Introduction

Possessing unique physical and chemical properties, diamond exhibits extremely high application potential in materials science, electrical engineering, and optical technology[1–3]. In the field of quantum information, nitrogen-vacancy (NV) centers in diamond have attracted widespread attention for quantum information science, nano magnetism, and biosensing owing to their outstanding optical, electronic spin, and quantum characteristics[4–6]. Furthermore, diamond NV centers enable optical initialization and readout as well as coherent control at room temperature or even higher temperatures via spin-dependent fluorescence, thereby allowing precise measurement of magnetic fields, electric fields, temperature, and pressure from the nanoscale to macroscopic regions[7,8]. In the field of micro-electro-mechanical systems (MEMS) and sensors, diamond-based high-Q mechanical resonators can be used for vibration metrology and pressure sensing, and NV center thermometers can also be integrated into single-crystal diamond MEMS resonators to achieve multi-mode thermal sensing[7,9]. It is precisely these unique properties that make the high-precision fabrication of diamond nanostructures one of the core challenges in current research.

In diamond micro- and nano-fabrication technology, despite its extreme physical performance, focused ion beam (FIB) technology can still achieve relatively controllable micro- and nano-machining[10–12]. However, although FIB milling is one of the most commonly used methods in micro- and nano-electronic device fabrication, it inevitably results in ion source material implantation and the formation of a damaged layer tens of nanometers thick, which is often overly severe for modern micro- and nano-electronic devices[13,14]. Specifically, during FIB milling, momentum transfer from ions to target atoms exceeding a critical dose leads to the amorphization of diamond within the ion interaction region[10,15]. For gallium-based FIB milling, a large amount of implanted gallium ions enriched in the damaged layer. Studies show that this damaged layer exhibits a bilayer structure, consisting of an a-C I layer primarily composed of sp^2-hybridized carbon atoms and an a-C II layer primarily composed of sp^3-hybridized carbon atoms[10,13]. In addition, while FIB technology can achieve precise fabrication of two-dimensional nanostructures, the surface amorphization and ion implantation it induces limit its usage in high-precision application scenarios such as size-effect studies[16,17].

To overcome the surface damage issues introduced by Ga-FIB processing, researchers have attempted various post-processing methods, among which helium ion microscopy (HIM) has garnered increasing attention due to its unique advantages[18,19]. The latest commercialized helium ion microscopes have demonstrated exceptional imaging capabilities in terms of resolution, surface sensitivity, depth of field, and charge compensation convenience[20]. HIM possesses the unique capability to directly mill arbitrary patterns, enabling the fabrication of sub-10 nm feature sizes[21,22]. However, systematic studies on the quantitative relationship between HIM processing parameters for diamond nanostructures (such as dose and beam current) and the thickness of the surface damaged layer remain relatively scarce, and the potential of multi-step step-down HIM processing strategies in minimizing the FIB damaged layer has not yet been fully explored. Fig. 1 illustrates the process of microstructural modification using FIB and HIM.

In view of this, this work systematically investigates the regulatory effect of focused helium ion beam post-processing on the surface damaged layer of single-crystal diamond structures after Ga-FIB milling. Centered on cross-sectional

transmission electron microscopy (TEM) quantitative characterization, combined with energy-dispersive X-ray spectroscopy (EDS), selected area electron diffraction (SAED), and high-resolution transmission electron microscopy (HRTEM) analysis, this paper focuses on examining the effects of HIM processing dose variations on the damaged layer of diamond nanostructures, the effects of HIM processing beam current variations on the damaged layer, and the practical thinning efficacy of a multi-step layer-by-layer decreasing HIM processing strategy based on low beam current and low dose. The research results aim to provide a parameter optimization basis for the high-quality manufacturing of diamond nanostructures and offer theoretical and experimental references for the design of FIB post-processing techniques.

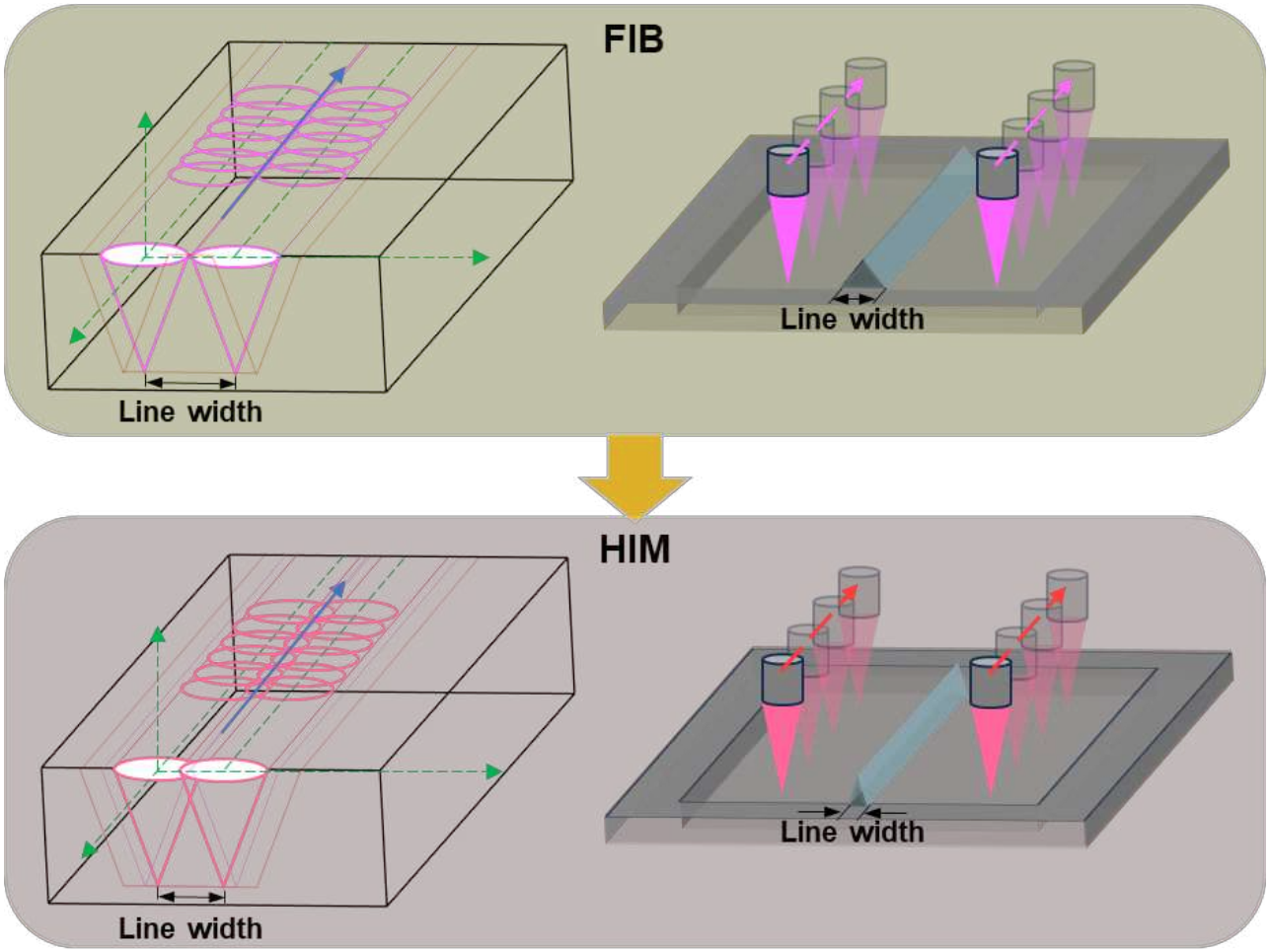


Fig. 1 Schematic diagram of diamond fabrication via FIB-HIM hybrid machining method

2. Materials and Methods

2.1 Diamond Substrate Preparation

A single-crystal (100) diamond substrate (3 × 3 × 1 mm³, double-side polished) was used. The sample was ultrasonically cleaned in acetone, absolute ethanol and deionized water for 5 min each and dried under nitrogen.

2.2 Focused Gallium Ion Machining Method

Two types of diamond nanostructures were fabricated on the diamond surface using the FIB machining component of the FIB-SEM system. One type was formed by machining rectangular grooves on the diamond. As shown in Fig.2a, the Rectangle Pattern scanning mode was selected in the FIB software, and the pattern to be machined was drawn. For this pattern,

parameter a was 3 μm, b was 11 μm, c was 1.5 μm / 2 μm, d was 10 μm, and the target machining depth e was 5 μm. The other type was formed by machining a single-sided taper on the diamond, with the diamond nanostructure created in the middle. As shown in Fig. 2b, the Single Taper Milling mode was selected in the FIB software, and the pattern to be machined was drawn. For this pattern, parameter a was 2 μm, b was 2 μm, and the target maximum machining depth e was 10 μm. For the FIB processing parameters, a liquid metal gallium ion source was selected, with an acceleration voltage of 30 kV and a beam current of 1 nA. An S-shaped scanning path was adopted, with the number of scans being 1000 for all cases. The incident angle was 0°, the pixel overlap rates in both X and Y directions were 50%, and the dwell time was 1 μs.

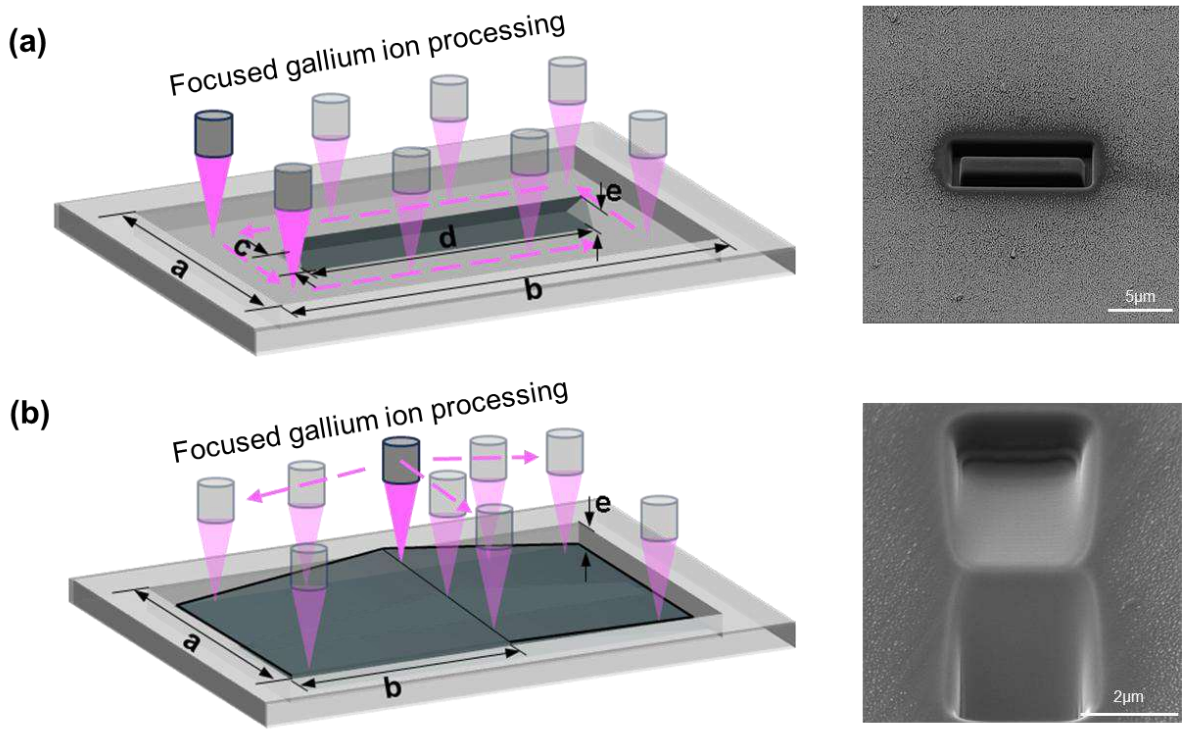


Fig. 2 FIB Processing Schematic Diagram (a) Rectangle Pattern scanning. (b) Single Taper Milling mode.

2.3 Focused Helium Ion Machining Method

Helium ion microscopy (HIM) was employed to thin the surface damage layer of the diamond nanostructures. As shown in Fig. 3a, different processing parameters were applied to regions I, II, and III in the dose experiment, whereas regions IV, V, and VI were left untreated. As shown in Fig. 4a, different processing parameters were utilized for regions I, II, and III in the beam current experiment, while regions IV, V, and VI shared the same parameters. As shown in Fig. 5a, different processing parameters were employed across regions I, II, III, and IV in the layer-by-layer decreasing experiment. Regarding the HIM processing parameters, the accelerating voltage was set to 30 kV, the incidence angle was 0°, the pixel overlap in both the X and Y directions was 50%, and the dwell time was 1 μm.

2.4 TEM specimen preparation

In this study, TEM lamellae of diamond nanowires were fabricated using a FIB-SEM system. The fabrication process consisted of five stages: Pt protective layer deposition, rough ion beam milling, in-situ lift-out, fine milling, and polishing, ultimately yielding TEM lamellae with a thickness of less than 100 nm.

First, a Pt protective layer of 2–3 μm in thickness was deposited on the target region at an accelerating voltage of 30 kV and a beam current of 0.3 nA. Deep trenches were then cut on both sides of the target region to form a suspended lamella. Rapid material removal was conducted using the FIB operating at an accelerating voltage of 30 kV and a beam current of 2–5 nA to reduce the sample thickness to 1–2 μm. Next, the sample was attached to a nanomanipulator and welded in place via Pt deposition. The bottom and sides of the lamella were severed using the FIB to detach the sample from the diamond substrate, and the sample was subsequently transferred to a copper grid. It was then welded to the copper grid using Pt deposition, after which the connection between the nanomanipulator and the sample was cut. Afterward, the sample was adjusted to the eucentric height, and layer-by-layer milling was performed by progressively decreasing the beam current (from 500 pA to 100 pA) to reduce the thickness to below 100 nm. Finally, low-energy FIB polishing was carried out at an accelerating voltage of 2–5 kV and a beam current of 10–50 pA to minimize the ion-implantation damage layer, ensuring that the sample thickness was controlled below 100 nm and yielding a high-quality TEM observation region.

3. Results and Discussion

3.1 Focused helium ion beam machining

3.1.1 Effect of helium ion beam dose on the damaged layer of diamond

Due to the relatively large mass of gallium ions, certain damages and dimensional errors are unavoidable during the FIB machining process, which may affect the surface quality of nanostructure and the performance of devices. In contrast, helium ions have a smaller mass and HIM has a smaller beam spot size, resulting in less damage during its machining process[23]. Meanwhile, HIM can provide higher spatial resolution, making it suitable for detailed machining at the nanoscale.

To optimize the fabricated nanostructures, HIM was used to thin the surface damage layer of diamond nanostructures induced by FIB machining and repair the nanostructure surface. By optimizing HIM machining parameters, the thickness of the damage layer on the diamond nanostructure surface was minimized, ensuring the fabrication of high-quality nanostructures. Regarding the effect of varying HIM machining doses on the damage layer, Fig. 3a shows the specific operation process. Since excessively high machining doses can cause severe damage to the substrate, FIB was first used to fabricate nanostructures with a single-sided conical shape (as illustrated in the figure). These fabricated nanostructures were then divided into six regions, denoted as I, II, III, IV, V, and VI. Subsequently HIM with different doses was applied to the divided regions for nanostructure machining the machining doses for Regions III II and I were 5×10^{15} ions/cm² 1×10^{16} ions/cm² and 3×10^{16} ions/cm² respectively while the dose for the remaining regions was 0 ions/cm².

Building on the nanostructure fabrication process described above, morphological analysis of the fabricated diamond nanostructures was conducted using energy-dispersive X-ray spectroscopy (EDS), selected area electron diffraction (SAED), and high-resolution transmission electron microscopy (HRTEM) – all performed via TEM. Fig. 3b presents the EDS mapping results of Region III in the TEM sample, where the red color represents carbon, green represents tungsten, and blue represents gallium. Based on the differences in enriched elements and their contents, Region III can be divided into four sub-regions:

①, ②, ③, and ④. Sub-region ① is the tungsten-enriched area, corresponding to the tungsten protective layer deposited during TEM sample preparation to safeguard the target region. Sub-region ② is the gallium-enriched area, formed by gallium ions implanted into the diamond surface during FIB machining and cutting. This sub-region has a relatively low carbon content and constitutes the fully amorphous layer within the surface damage layer of the diamond nanostructure. Sub-region ③ is the lattice damage layer. The carbon distribution obtained from EDS provides information on the elemental composition of the investigated region but cannot directly quantify the degree of lattice disorder or amorphization. Variations in the carbon signal were observed across the investigated regions. However, these variations alone cannot be used to determine the degree of lattice damage. Therefore, the structural characteristics of the damaged layer were further examined using HRTEM and electron diffraction analyses. Sub-region ④ is the carbon-enriched area, representing the undamaged crystalline layer of the diamond. Each sub-region in the figure exhibits a clear layered structure the thickness of Sub-region ② is approximately 39.66 nm and that of Sub-region ③ is about 153.31 nm. Together, Sub-regions ② and ③ form the main damage layer. Meanwhile, the figure clearly demonstrates the typical gradient structure of the diamond surface after focused ion beam machining, transitioning from the amorphous layer, through the lattice damage layer, to the intact crystalline layer[24]. Furthermore, EDS line scanning of Region III (Fig. 3c) was conducted, which further confirms the aforementioned identification of the four sub-regions (①, ②, ③, and ④).

Fig. 3d shows the SAED analysis result of Region III. The figure displays clear diffraction lattices accompanied by diffraction rings, indicating that the sample still retains a certain crystalline structure but may contain microcrystals or local strains. However, there are strong diffuse rings in the background, suggesting that the surface of the sample may have partial amorphization or defect-induced diffraction diffusion. This diffraction pattern demonstrates that the diamond nanostructure as a whole still maintains the diamond crystal structure, but there is a certain damage layer on its surface, which consists of an amorphous layer and a lattice damage layer.

Fig. 3e shows the HRTEM image of Region III. Due to the excessive thickness of the damage layer, it could not be fully captured in a single HRTEM image, necessitating segmented imaging of the damage layer. The HRTEM images further reveal the microstructural evolution characteristics of the diamond nanostructure surface layer. From the surface to the interior, the integrity of the crystal structure gradually changes at different depths. The surface layer consists of an amorphous layer formed by gallium ion implantation, featuring disordered atomic arrangement and containing a small amount of nanocrystals. The middle layer represents the deep damage layer processed by gallium ions, exhibiting partial lattice order. The deep layer approaches a complete diamond crystal lattice[25].

To further verify the effect of HIM machining doses on the damage layers of diamond, EDS mapping analysis via TEM was also performed on different regions (Fig. 3f). As observed in the figure, the carbon content in Sub-region ③ (lattice damage layer) varies across different regions. The carbon content in Sub-region ③ of Region III is lower than that in Sub-region ③ of Region IV, the carbon content in Sub-region ③ of Region II is lower than that in Sub-region ③ of Region V, and the carbon content in Sub-region ③ of Region I is lower than that in Sub-region ③ of Region VI. These observations

indicate that different HIM machining doses lead to varying degrees of damage and amorphization in the lattice damage layer of diamond nanostructures. This further verifies that an appropriate helium ion beam dose can effectively thin the surface damage layer of diamond nanostructures.

To more specifically characterize the thickness of the damage layer formed by different HIM machining doses, the thicknesses of the damage layers in different regions were measured with HRTEM images as the reference, and the results are listed in Table 1. Among these regions, the damage layer thickness of Region III is approximately 192.97 nm, which is significantly smaller than that of Regions IV, V, and VI, regions that underwent focused ion beam (FIB) machining but no HIM machining. This indicates that HIM machining can reduce the thickness of the damage layer caused by FIB machining. Meanwhile, the damage layer thicknesses of Regions I and II are 215.54 nm and 205.62 nm, respectively, which are significantly larger than those of Regions III, IV, V, and VI. This demonstrates that different HIM machining doses lead to different degrees of damage. A relatively high dose not only fails to reduce the damage layer but also further increases the damage degree of diamond.

In summary, an appropriate helium ion beam dose has the effect of effectively thinning the surface damage layer of diamond nanostructures.

Table 1 Thickness of HIM Damage Layer with Changed Doses

region	dose/(ions/cm^2)	thickness /(nm)	region	dose/(ions/cm^2)	thickness /(nm)
I	$3*10^{16}$	215.54 ± 0.36	IV	0	200.39 ± 1.46
II	$1*10^{16}$	205.62 ± 0.97	V	0	197.18 ± 0.42
III	$5*10^{15}$	192.97 ± 1.06	VI	0	203.18 ± 0.89

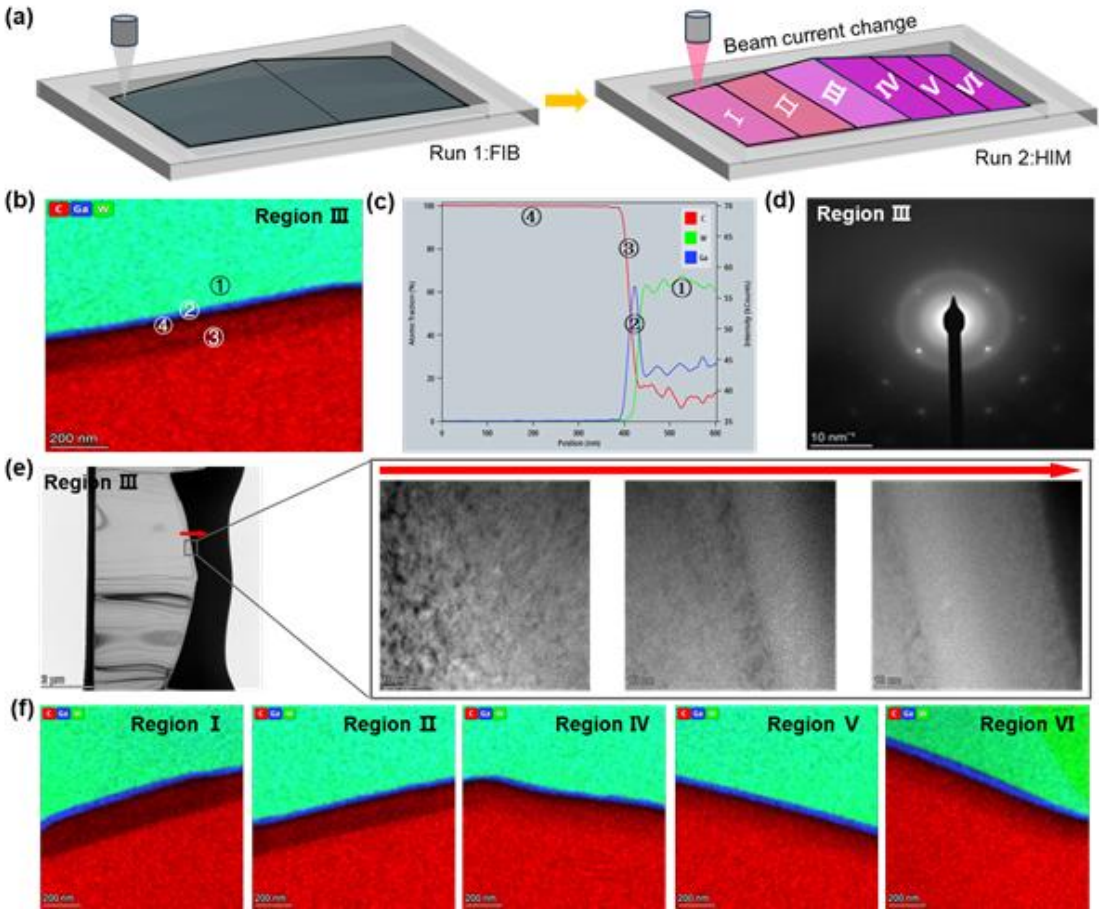


Fig. 3 HIM Dose Optimization Diagrams(a) HIM dose optimization experimental process. (b) EDS mapping image of Region III. (c) EDS line scan image of Region III. (d) SAED image of Region III. (e) High-resolution image of Region III. (f) EDS Mapping Images of Different Regions.

3.1.2 Effect of helium ion beam current on the damaged layer of diamond

Subsequently, discussions were conducted on another important influencing factor of HIM machining, namely the effect of beam current variation on the damage layer. The specific experimental process is essentially consistent with the aforementioned experiment involving dose variation. As shown in Fig. 4a, the fabricated nanostructure was divided into six regions (I, II, III, IV, V, and VI), and different regions were machined using focused helium ion beams with different beam currents. Among these regions, the beam currents applied to Regions III, II, and I were 29.67 pA, 20 pA, and 13 pA, respectively, while the beam current for Regions IV, V, and VI was 12 pA.

Consistent with the aforementioned procedures, EDS, SAED, and HRTEM analyses were performed on Region III of the fabricated nanostructures using transmission electron microscopy (TEM). Fig. 4b shows the EDS mapping result of Region III, and Fig. 4c presents the EDS line scan result of Region III, where the red color represents carbon, green represents tungsten, and blue represents gallium. From the structural layering in the EDS mapping result, Region III can still be divided into four sub-regions (①, ②, ③, and ④). The division of these four sub-regions is consistent with the aforementioned explanation, which is based on the degree of damage. Sub-region ① is the tungsten protective layer. Sub-region ② is the amorphous layer on the surface of the diamond nanostructure, with a thickness of approximately 47.37 nm. Sub-region ③ is the lattice damage layer, with a thickness of about 126.04 nm. Sub-region ④ is the diamond crystalline layer. Sub-regions ② and ③

together constitute the main part of the damaged area. It can be seen from the figures that the change in beam current also has a certain impact on diamond damage, and the degree of influence of beam current on diamond damage is greater than that of dose on the damage layer. Meanwhile, the typical gradient structure, from the amorphous layer, through the lattice damage layer, to the intact crystalline layer, can be clearly observed in the figures. Similarly, the EDS line scan result of Region III (Fig. 4c) confirms the aforementioned identification of the four sub-regions (①, ②, ③, and ④). Fig. 4d displays the SAED analysis result of Region III. Certain diffraction lattices and diffused diffraction rings are present in this image, indicating that there is a damage layer containing a certain amorphous layer on the surface of the diamond nanostructure, while the interior of the diamond remains in a crystalline structure. Fig. 4e is the HRTEM image of Region III, which reveals the microstructural evolution characteristics of the diamond nanostructure's surface layer. From the surface layer to the interior, the integrity of the crystal structure gradually changes at different depth positions.

The aforementioned conclusion is further verified through EDS mapping analysis (via TEM) of different regions (Fig. 4f). In the figure, by comparing the carbon content in Sub-region ③ and the thickness of the amorphous layer across different regions, it can be clearly observed that the amorphous layer thicknesses of Regions I, II, and III are greater than those of Regions IV, V, and VI. All regions processed at 13–29.67 pA exhibited thicker local damaged layers than their corresponding 12 pA reference regions. However, the thickness did not vary monotonically with beam current. Thus, it is verified that an appropriate helium ion beam current can effectively modify the surface damage layer of diamond nanostructures.

Similarly, with HRTEM as the reference, the thickness of the damage layer in different regions was measured, and the specific thicknesses of the damage layer under different beam current conditions are listed in Table 2. It can be seen from the table that the damage layer thicknesses of Regions I, II, and III are 164.5 nm, 183.7 nm, and 173.41 nm respectively, all of which are higher than those of Regions IV, V, and VI. This indicates that an excessively large beam current cannot thin the damage layer. When the beam current is too large, helium ions are densely implanted in a short period to form an aggregation area, which reduces the recrystallization ability. At the same time, the high energy density is likely to penetrate into deeper regions, which instead thickens the damage layer and causes surface bulging[23]. In summary, during the HIM machining process, on the basis of ensuring the machining effect, the beam current should be reduced as much as possible.

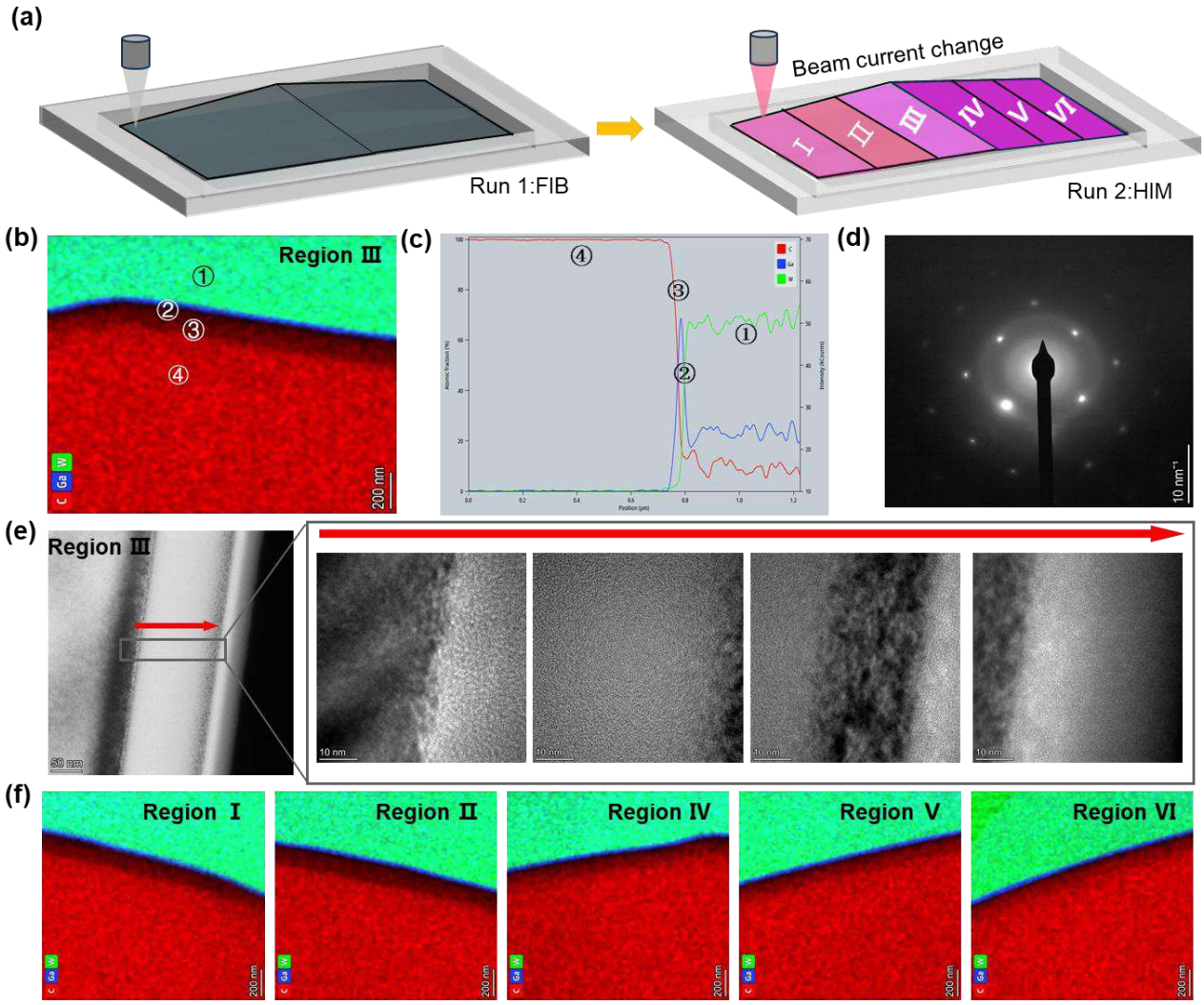


Fig. 4 HIM Beam Current Optimization Diagrams(a) HIM beam current optimization experimental process. (b) EDS mapping image of Region III. (c) EDS line scan image of Region III. (d) SAED image of Region III. (e) High-resolution image of Region III. (f) EDS Mapping Images of Different Regions.

Table 2 Thickness of HIM Damage Layer with Changed Beam current

region	beam current/(pA)	thickness /(nm)	region	beam current/(pA)	thickness /(nm)
I	13.00	164.50± 0.07	IV	12.00	144.79± 1.74
II	20.00	183.70± 0.95	V	12.00	143.39 ± 1.37
III	29.67	173.41± 0.34	VI	12.00	139.18 ± 1.98

3.2 Focus on helium ion beam layer-by-layer decreasing machining

In the actual experimental process, when the dose and beam current are changed simultaneously, the damage layer thinned by the HIM exhibits significant fluctuations. Furthermore, changes in small doses and small beam currents have a limited effect on reducing the damage layer, making it impossible to thin the damage layer induced by the FIB as much as possible. However, when the reduction in the damage layer achieved by small increments is accumulated multiple times, the resulting thinning of the damage layer fully meets the work requirements. Meanwhile, during the multiple focused helium ion machining processes, in addition to adjusting the dose and beam current, adjustments can also be made to the shape and surface morphology of the nanostructures.

In this work, during HIM machining, the method of FIB thinning the amorphous layer was mimicked, and a helium ion beam with low dose/low beam current was used to machine diamond nanostructures in a layer-by-layer decreasing manner.

Fig. 5a shows the specific process of the six thinning cycles, where two rectangles fabricated by FIB were treated with different doses and beam currents respectively. Meanwhile, the rectangular grooves were divided into regions. Regions Ⅱ and Ⅳ were machined by HIM in a layer-by-layer decreasing mode (detailed parameters are listed in Table 3), while Regions Ⅰ and Ⅲ were not subjected to HIM machining. Scanning electron microscopy (SEM) was used to characterize the nanostructures before and after machining (Fig. 5a (i) and (ii)). Significant differences between the nanostructures after FIB machining and HIM machining can be clearly observed in the figures. The nanostructures after HIM machining are more regular and cleaner.

Subsequently, the aforementioned consistent analytical procedures were performed on the post-machining nanostructures. TEM was used to conduct EDS, SAED, and HRTEM analyses on the surface morphology of Region Ⅱ of the fabricated nanostructures. Fig. 5b shows the EDS mapping result of Region II, and Fig. 5c presents the EDS line scan result of Region II, where red represents carbon, green represents tungsten, and blue represents gallium. It can be observed from the figures that after multiple HIM thinning operations, the thickness of the diamond's damage layer is effectively reduced compared to that after the aforementioned single HIM machining. Specifically, the amorphous layer on the diamond nanostructure surface has a thickness of approximately 17 nm, and the lattice damage layer has a thickness of about 4 nm. Additionally, the diamond nanostructure still exhibits the typical gradient structure, transitioning from the amorphous layer, through the lattice damage layer, to the intact crystalline layer. Fig. 5d displays the SAED analysis result of Region II. Only diffraction lattices (and no amorphous rings) are observed in this image, indicating minimal surface damage to the diamond. Fig. 5e is the HRTEM image of Region II, and images of other regions were captured using the same method. With HRTEM images as the reference, the damage layer thicknesses of different regions are listed in Table 4. As shown in the table, the damage layer thicknesses of Regions I and III (subjected to multiple HIM machining cycles) are 23.17 nm and 26.30 nm, respectively. In contrast, the damage layer thicknesses of Regions II and IV (subjected to FIB machining but no HIM machining) are 21.87 nm and 24.2 nm, respectively. Regions II and IV underwent six-pass He^+ ion-beam post-processing, whereas Regions I and III served as the corresponding Ga-FIB-only controls. The local damaged-layer thickness decreased from 23.17 ± 0.17 nm in Region I to 21.87 ± 0.82 nm in Region II, corresponding to a reduction of 1.30 nm (5.6%). Similarly, the thickness decreased from 26.30 ± 0.06 nm in Region III to 24.20 ± 0.10 nm in Region IV, corresponding to a reduction of 2.10 nm (8.0%). Furthermore, the aforementioned conclusion is further verified through EDS mapping analysis of different regions (Fig. 5f).

In summary, due to the very shallow penetration depth of helium ions in diamond, they generally only affect the surface layer of a few nanometers thick. Machining layer by layer with small doses and low beam currents enables more precise removal of the surface damage layer. The weak interaction between low-energy helium ions and carbon atoms facilitates the rearrangement of the surface structure, induces local self-healing, and reduces new damage[24]. Compared with one-time machining using large doses and high beam currents, this method allows better control over the thickness of the damage layer and avoids the formation of bubbles or excessive damage. It can remove the original damage while reducing new damage, providing a more optimal approach for the post-processing of diamond nanostructures. Additionally, it enhances the

controllability of diamond nanostructure fabrication and makes the production of high-quality diamond nanostructures possible.

Table 3 Parameters for Multiple HIM Machining Processes

Region II: Processing sequence	beam current /pA	dose /(ions/cm^2)	Region IV: Processing sequence	beam current /pA	dose /(ions/cm^2)
1	3.6	$3.9*10^{14}$	1	3	$5*10^{14}$
2	3.1	$3.8*10^{14}$	2	3	$3*10^{14}$
3	2.6	$3.9*10^{14}$	3	3	$1*10^{14}$
4	2.0	$3.8*10^{14}$	4	3	$7*10^{13}$
5	1.6	$3.9*10^{14}$	5	3	$5*10^{13}$
6	1.1	$4.0*10^{14}$	6	3	$2*10^{13}$

Table 4 Damage Layer Thickness After Multiple HIM Processes

region	thickness /nm	region	thickness /nm	reduction/(nm)	reduction/(%)
I	23.17 ± 0.17	II	21.87 ± 0.82	1.30	5.6%
III	26.30 ± 0.06	IV	24.20 ± 0.10	2.10	8.0%

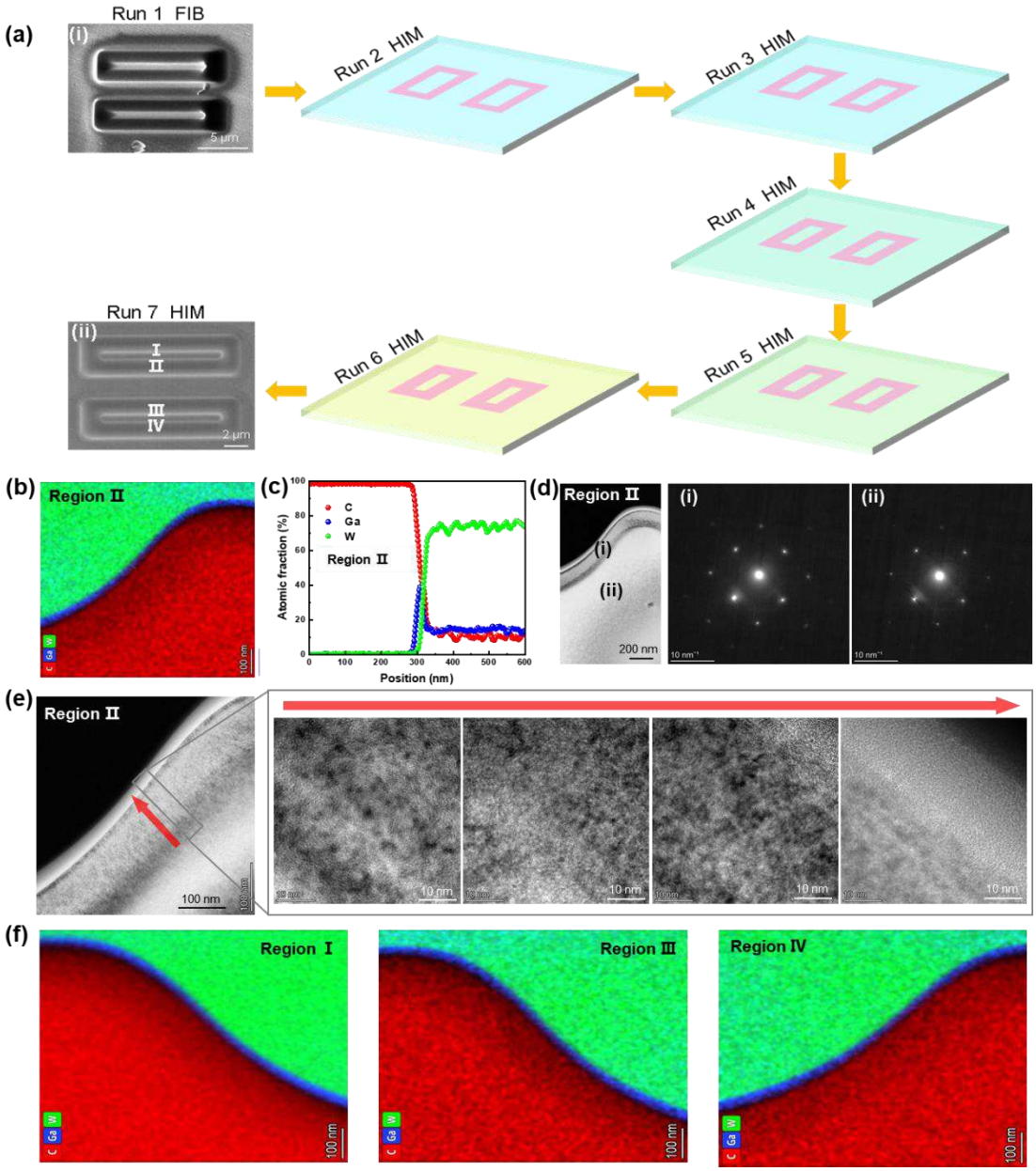


Fig. 5 HIM Cycle Optimization Diagrams(a) HIM cycle optimization experimental process, where (i) and (ii) are images of the TEM sample before and after fabrication. (b) EDS mapping image of Region II. (c) EDS line scan image of Region II. (d) SAED image of Region II. (e) High-resolution image of Region II. (f) EDS Mapping Images of Different Regions.

4.Conclusion

This work investigated focused helium ion beam post-processing of Ga-FIB-milled single-crystal diamond structures with cross-sectional TEM quantification.

Ga-FIB milling produces a gradient near-surface damaged structure consisting of an amorphous region and a subsurface lattice-disordered region over crystalline diamond. In a dose series, 5×10^{15} ions/cm² produced a measurable local reduction in damaged-layer thickness (from 200.39±1.46nm to 192.97±1.06nm), whereas higher doses ($\geq1\times10^{16}$ ions/cm²) increased the damaged-layer thickness and were accompanied by swelling-like features. In a beam-current series, higher-current conditions (13–29.67 pA) resulted in thicker damaged layers than a 12 pA reference condition, although the thickness did not vary monotonically with current. Two six-pass step-down He-HIM strategies reduced damaged-layer thickness in paired comparisons by 5.6% and 8.0%, demonstrating that low-current multi-pass processing provides a practical route for damage

regulation in FIB-machined diamond structures.

Overall, He-HIM post-processing is not universally beneficial; it is governed by competition between removal of pre-existing FIB damage and additional helium-induced irradiation damage. Controlled low-current, multi-pass processing is therefore recommended for minimizing near-surface damage.

Acknowledgements

This research was funded by General Program (52175388) funded by the National Natural Science Foundation of China.

Competing interests

The authors declare no competing interests.

Reference

[1] Zhang R, Peng N, Ye H. A perspective on diamond heterojunction devices. Appl. Phys. Lett. 2025;127(7):070501.

[2] Koide Y. Diamond and iii-nitride wide-bandgap semiconductors: a research journey. Funct. Diam. 2025;5(1):2554126.

[3] Schirhagl R, Chang K, Loretz M, et al. Nitrogen-vacancy centers in diamond: nanoscale sensors for physics and biology. Annu. Rev. Phys. Chem. 2014;65:83–105.

[4] Yang N, Krueger A, Hamers RJ. Diamond chemistry: advances and perspectives. Angew. Chem. 2025;64(25):e202418683.

[5] Yang H, Ma Y, Dai Y. Progress of structural and electronic properties of diamond: a mini review. Funct. Diam. 2022;1(1):150–159.

[6] Li Y, Li H, Yi T, et al. A review of the study of diamond nv color centers: fabrication, application and challenge. Funct. Diam. 2025;5(1):2567286.

[7] Yip PS, Zhao T, Guo K, et al. Diamond sensor technologies: from multi stimulus to quantum. Micromachines. 2026;17(1):118.

[8] Hayashi K, Matsuzaki Y, Taniguchi T, et al. Optimization temperature sensitivity using the optically detected magnetic resonance spectrum of a nitrogen-vacancy center ensemble. Phys. Rev. Appl. 2018;10(3):034009.

[9] Zhang Z, Gu K, Chen G, et al. Electrical actuation of single-crystal diamond mems resonators at high temperatures. Funct. Diam. 2024;4(1):2346085.

[10] Yang Y, Wang Q, Chen L, et al. Orientation-dependent effects in single-crystal diamond during focused gallium ion beam processing. Diam. Relat. Mater. 2025;158:112631.

[11] Graziosi T, Mi S, Kiss M, et al. Single crystal diamond micro-disk resonators by focused ion beam milling. APL Photonics. 2018;3(12):126101.

[12] Choi WK, Baek SY. Study on platinum coating depth in focused ion beam diamond cutting tool milling and methods for removing platinum layer. Materials. 2015;8(9):6498–6507.

[13] Jia G, Chen G, Zhang L, et al. Study of amorphous layer on cvd diamond surface induced by ga ion implantation in focused ion beam processing. Diam. Relat. Mater. 2024;145:111108.

[14] Rubanov S, Suvorova A. Ion implantation in diamond using 30 kev ga+ focused ion beam. Diam. Relat. Mater. 2011;20(8):1160–1164.

[15] Martin AA, Randolph S, Botman A, et al. Maskless milling of diamond by a focused oxygen ion beam. Sci. Rep. 2015;5(1):8958.

[16] Hofmann F, Tarleton E, Harder RJ, et al. 3D lattice distortions and defect structures in ion-implanted nano-crystals. Sci. Rep. 2017;7:45993.

[17] Stanishevsky A. Focused ion beam patterning of diamondlike carbon films. Diam. Relat. Mater. 1999;8(7):1246–1250.

[18] Nano-structuring, surface and bulk modification with a focused helium ion beam. Beilstein J. Nanotechnol. 2012;3:579–585.

[19] Joens MS, Huynh C, Kasuboski JM, et al. Helium ion microscopy (him) for the imaging of biological samples at sub-nanometer resolution. Sci. Rep. 2013;3:3514.

[20] Schmidt M, Byrne JM, Maasilta IJ. Bio-imaging with the helium-ion microscope: a review. Beilstein J. Nanotechnol. 2021;12:1–23.

[21] Allen FI. A review of defect engineering, ion implantation, and nanofabrication using the helium ion microscope. Beilstein J. Nanotechnol. 2021;12:633–664.

[22] Mo S, Byrne DO, Allen FI. Focused helium ion beam nanofabrication by near-surface swelling. J. Vac. Sci. Technol. B. 2025;43(2):022803.

[23] Kim C-S, Hobbs RG, Agarwal A, et al. Focused-helium-ion-beam blow forming of nanostructures: radiation damage and nanofabrication. Nanotechnology. 2020;31(4):045302.

[24] Tang F, Chen Y, Zhang L. Analysis of polished polycrystalline diamond using dual beam focused ion beam microscopy. Philos. Mag. 2012;92(13):1680–1690.

[25] McKenzie WR, Quadir MdZ, Gass MH, et al. Focused ion beam implantation of diamond. Diam. Relat. Mater. 2011;20(8):1125–1128.